SUPPLEMENTAL INFORMATION

SUPPLEMENTAL DATA

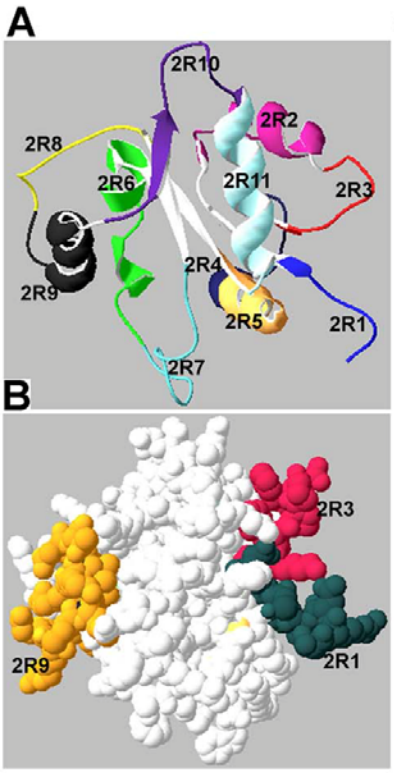

C

Sequences of decoy peptides

Peptide name	Peptides sequence	Predominant structural region
2R1	RKPKKAPCRDVCYD	Segment that precedes strand A
2R2	EQDSHWVENLMVQQ	A helix
2R3	ENSDPPFKLC	AB loop
2R34	PPFKLCLHKRDF	B strand and BB loop
2R4	HKRDFVPGKWIID	BB loop and B helix
2BB	LHKRDFVPGKWIID	BB loop and B helix
2R5	NIIDSIEKSHKT	B helix
2R6	ENFVRSEWCKYELD	C helix
2R7	FSHFRLFDENNDAA	CD loop
2R8	LLEPIERKAI	D strand and DD loop
2R9	PQRFCKLRKIMNT	DD loop and D helix
2R10	TYLEWPLDEGQQ	E strand and EE loop
2R11	EVFWVNLRTAIKS	E helix
MR4	SDRDVLPGTCVWS	BB loop (MyD88)
TR6	PGFLRDPWCKYQML	C helix (TIRAP)
CP	SLHGRGDPMEAFII	Random sequence

Figure S1. TLR2 regions that correspond to decoy peptides and the sequences of peptides. Related to Figure 1

(A) Regions of TLR2 TIR represented by decoy peptides.

(B) Regions represented by inhibitory peptides, 2R1 (dark green), 2R3 (red), and 2R9 (yellow) are highlighted. Images were produced using the DeepView viewer and PDB file 1FYW (Guex and Peitsch, 1997; Xu et al., 2000).

(C) TLR2 TIR peptides used in the primary screening are designated 2R1 - 2R11. Peptides TR6, MR4, 2BB, and CP were described previously (Couture et al., 2012; Toshchakov et al., 2005; Toshchakov et al., 2007) and represent C helix of TIRAP, BB loop of MyD88 and TLR2, and a random sequence, respectively.

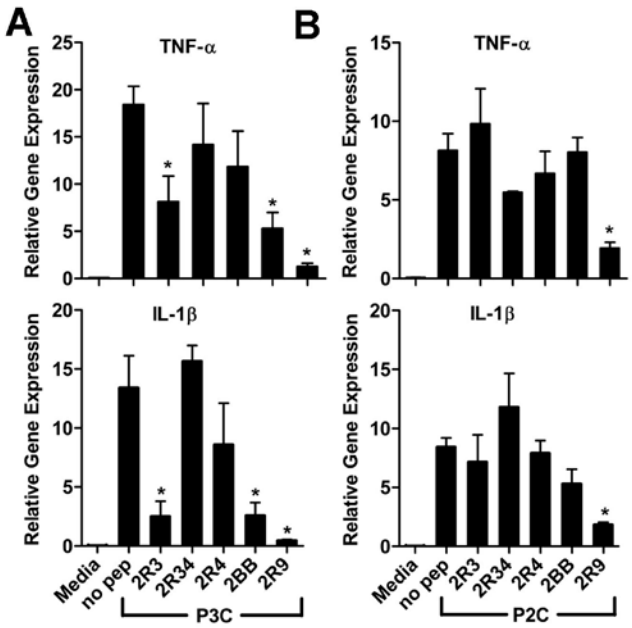

Figure S2. Effect of peptides derived from areas adjacent to strand B on TLR2-induced cytokine expression. Related to Figure 1

(A) Effect of peptides on P3C-induced cytokine expression. Experimental details are as described in the legend for Figure 1.

(B) Effect of peptides on P2C-induced cytokine expression.

Figure S2 exhibits the difference in inhibitory potency of highly similar 2R4 and 2BB peptides. Because TLR2 L647, amino acid which was included as the N-terminal residue of 2BB, the TLR2 BB loop peptide that we tested previously (Toshchakov et al., 2007), is not exposed to the surface in the TLR2 TIR domain (Xu et al., 2000), this residue was excluded from 2R4. Surprisingly, removal of N-terminal leucine negatively affected the inhibitory potency of 2BB, albeit slightly (Figure S2A). These findings together indicate that while Leu647 cannot mediate functional interactions of the folded TIR, its presence in the context of decoy peptide is important for 2BB binding to its targets. Leucine often enhances peptide-protein binding (London et al., 2010). Peptide centered on strand B of TLR2 (2R34) did not inhibit TLR2.

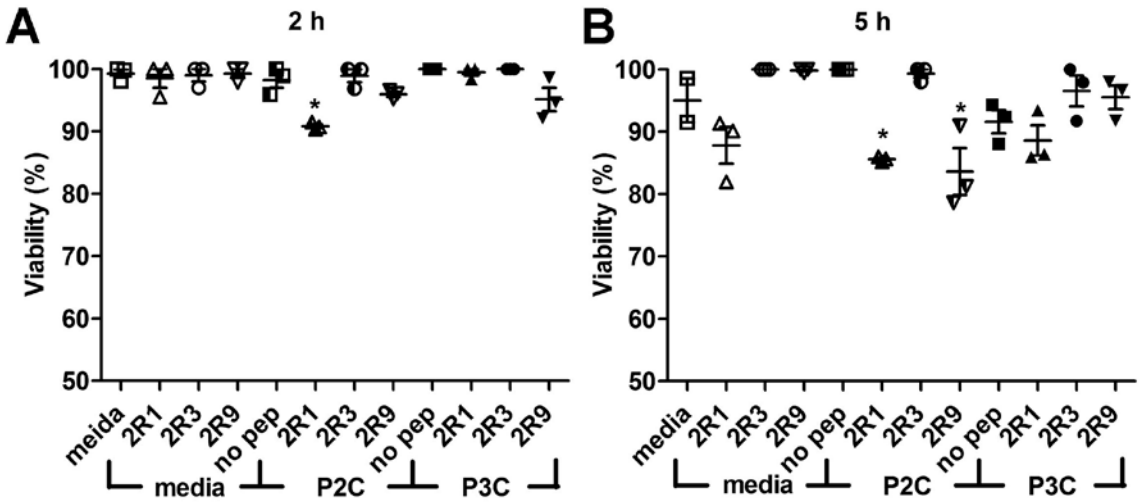

Figure S3. Effect of inhibitory peptides on cell viability. Related to Figure 1

(A-B) Mouse macrophages were incubated with TLR2 inhibitory peptides at 40 μM for 2 (A) or 5 hours (B) without or with stimulation with TLR2 agonists, P2C or P3C. Cell viability was determined using 3-[4,5-dimethylthiazol-2-yl]-2,5 diphenyltetrazolium bromide (MTT) incorporation assay. Data were collected in 3 independent experiments.

Although a slight, but statistically significant diminution of viability could be noted after 2 h incubation of P2C-stimulated cells in the presence of 2R1, the cell viability remained higher than 90% in all conditions tested (Figure S3A). Longer incubations affected cell viability to a greater extent, yet cell viability exceeded 80% at the end of the testing, even in the presence of 2R1. The 2R1- and 2R9-caused diminution of macrophage viability was not statistically different from the diminution caused by P3C stimulation of cells in the absence of peptides (Figure S3B).

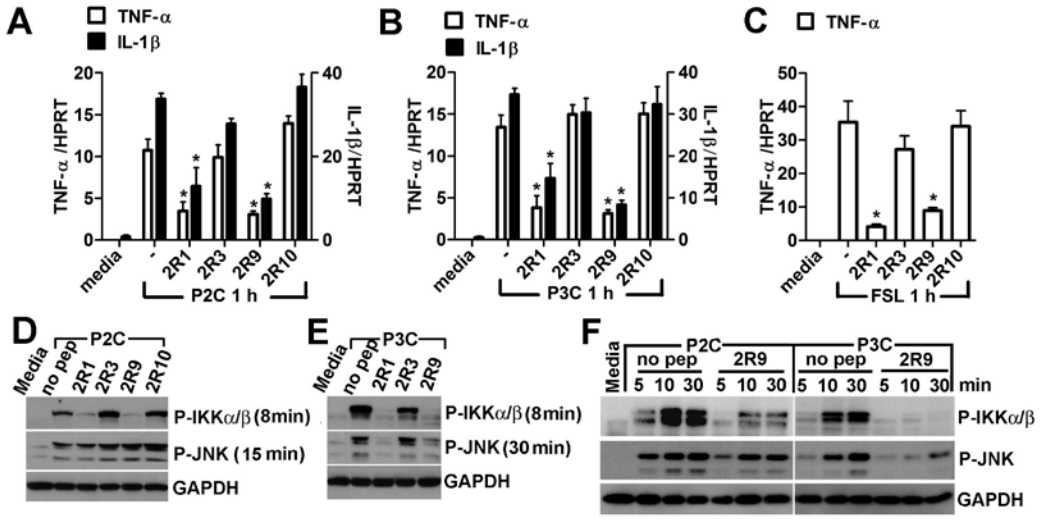

Figure S4. 2R1 and 2R9 inhibit TLR2-induced activation of human macrophages. Related to Figure 1

(A-C) THP-1 cells, differentiated by 10 nM PMA for 3 days, were treated with 40 μM of an indicated peptide for 30 min and stimulated with P2C (50 ng/ml), P3C (500 ng/ml) or FSL-1 (50 ng/ml). TNF-α and IL-1β mRNA expression was measured 1 h after stimulation of cells with an agonist. Means ± SEM of 4 individual experiments are shown.

(D-F) IKK-α/β and JNK phosphorylation analyzed by Western blotting.

2R1 and 2R9 potently inhibited TNF-α and IL-1β mRNA induced by P2C, P3C, or FSL-1 in THP-1 cells (Figure S4A-C). Both peptides also markedly inhibited IKK-α/β activation, regardless of which TLR2 agonist was used (Figure S4D-F). Highlighting the similarity of peptide action in human and mouse macrophages is that both 2R1 and 2R9 decreased JNK phosphorylation induced by P3C, but not by P2C in both murine and human cells (Figures 1D-F and S4D-F).

The region represented by 2R9 is identical in human and mouse TLR2. The 2R1 region is less conserved; in humans, it has 4 positive amino acid replacements compared to the same

region in the mouse protein (RKPRKAPSRNICYD, conserved amino acids in human 2R1 are underlined). Yet both 2R1 and 2R9 work similarly in human and mouse cells. These observations support the notion that sequence divergence of peptides or proteins, which demonstrate similar binding behavior, may vary substantially.

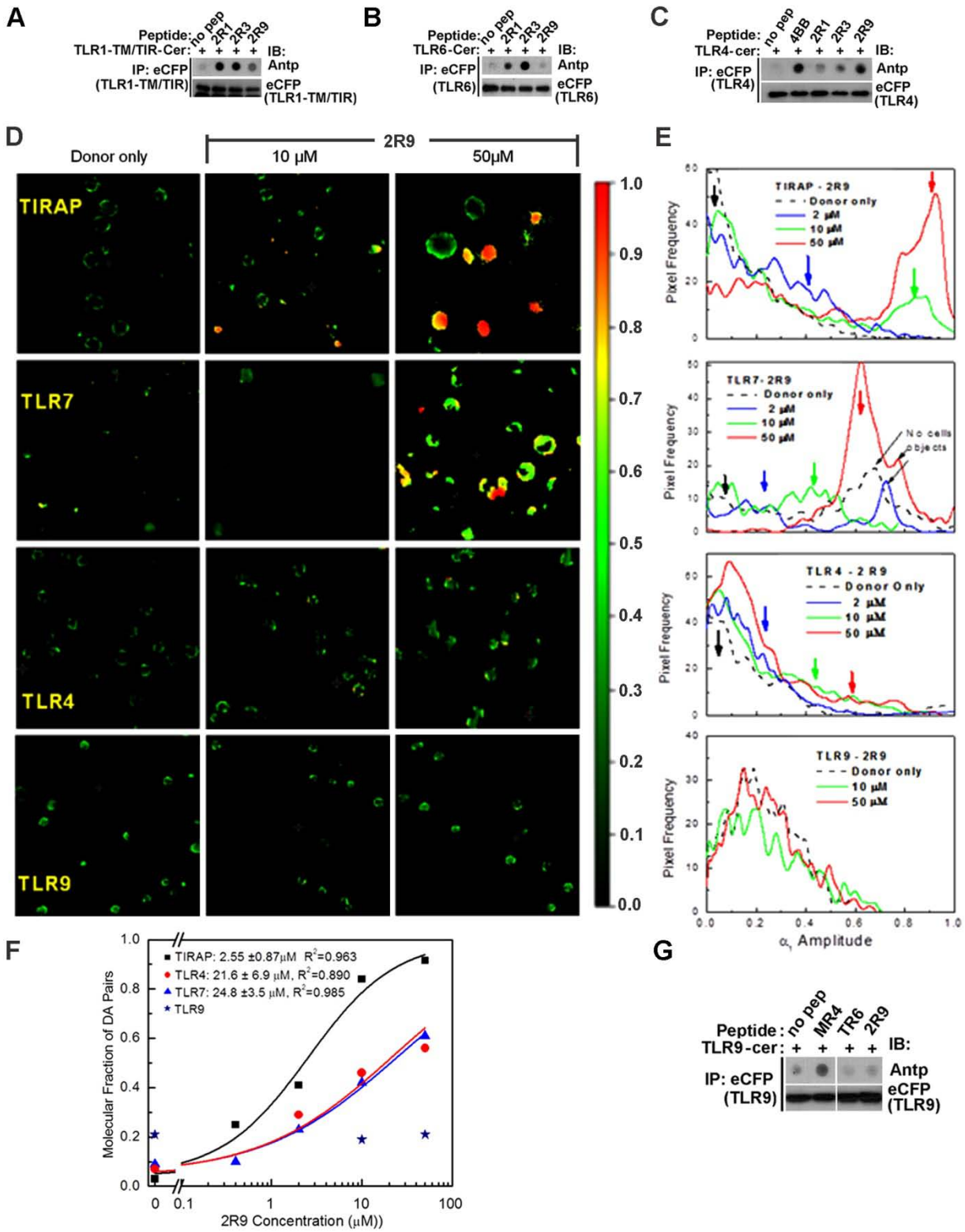

Figure S5. Binding of TLR2-derived peptides to TLRs. Related to Figure 3

(A-C) HEK 293T cells were transfected with a TLR-Cer expression vector and lysed two days

later. The lysates were supplemented with decoy peptides and TLRs immunoprecipitated with anti-CFP antibody. The precipitates were blotted and peptides quantified using antibody to the *Antennapedia* cell-permeating sequence present in each peptide. Representative blots for at least 3 independent experiments are shown.

(D) The short lifetime component amplitude-based images of HeLa cells transfected with indicated TIR-Cer vectors and mock-treated or treated with different concentrations of BTX-2R9 for one hour.

(E) Distribution of the apparent molecular fraction of acceptor-bound TIR domains for TIRAP-Cer-, TLR7-Cer-, TLR4-Cer-, and TLR9-Cer in FLIM images of HeLa cells incubated in the presence of different 2R9 concentration. The molecular fractions were calculated from characteristic amplitudes of lifetime components in cell images on the pixel-by-pixel basis.

(F) Concentration dependence of the apparent molecular fraction of acceptor-bound TIR domains for TIRAP-Cer-, TLR7-Cer-, TLR4-Cer or TLR9-Cer-expressing HeLa cells. The molecular fractions were calculated from characteristic amplitudes of lifetime components in images of cells incubated with different concentrations of acceptor.

(G) Dot blot measurements suggested no 2R9-TLR9 binding. Experiments were conducted as described in Figure S5A-C.

FLIM images and histograms in panels S5D and S5E confirm Figure 3 data that the short lifetime component amplitude, $\alpha 1$, of TIRAP-Cer fluorescence depends strongly on concentration of 2R9 (the upper row of images), indicating strong FRET due to direct 2R9-TIRAP binding. The images also suggested that there is a weaker quenching of TLR7-Cer and TLR4-Cer fluorescence by 2R9, manifested by the increased number of pixels with $\alpha 1>0.5$ in images in the presence of 2R9. It should be noted that the quantitative analysis of 2R9 binding

to TLR7 and TLR4 TIR domains was complicated by significantly different expression of these transfected proteins. Expression of TLR7 was particularly weak despite similar type of vector and transfection conditions were used for all TIR-Cer fusion proteins. Low expression of TLR7-Cer required significantly higher intensity of excitation and, consequently, more careful analysis of images to exclude artificial objects that appeared in the TLR7 images due to high laser intensity. Artificial signals in TLR7 images that do not correspond to Cer-expressing cells (Figure S5E) were excluded based on analysis of their shape and also fluorescence intensity, spectrum, and lifetime. Based on analysis of several images we concluded that the 2R9 binding affinity to TLR7 and TLR4 TIR domains is approximately 10 times lower than that for TIRAP (Figure S5F). FRET-FLIM and dot blot analyses detected no signs of 2R9 binding to TLR9 despite slightly lower levels of expression of TLR9 compared to TLR4 in host cells (Figure S5D-G). It should be noted that expression of Cer fusion proteins analyzed in Figure 3, TIRAP, TLR1 and MyD88 TIR, did not differ significantly.

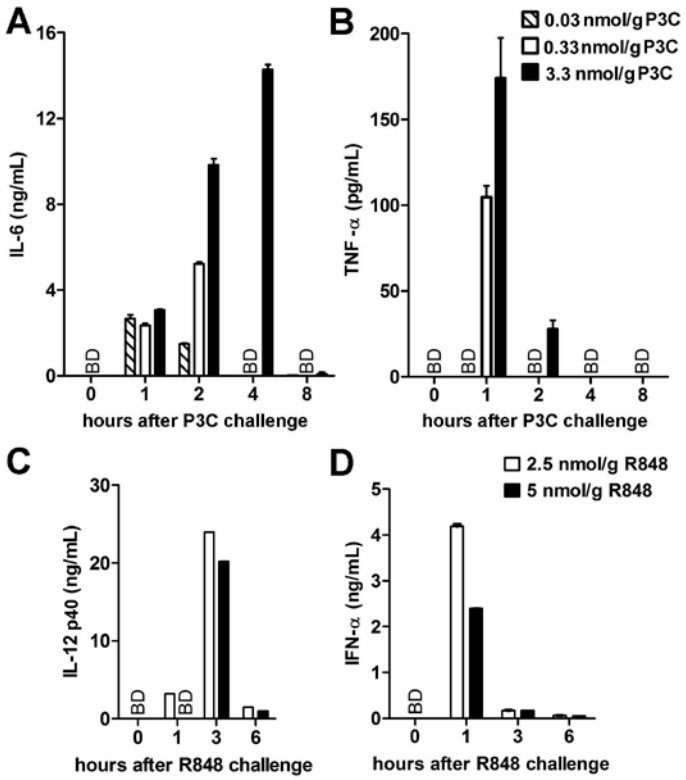

Figure S6. Systemic cytokine levels following i.p. administration of P3C (A, B) or R848 (C, D) to C57BL/6J mice. Related to Figure 5

To determine the optimize dose of TLR agonists to be used in evaluation of 2R9 potency *in vivo*, we first studied the dose dependence of systemic cytokine response induced in mice by a single i.p. administration of a purified TLR2 or TLR7 agonist. We found that P3C at the dose of 3.3 nmol/g of mouse weight induces a strong systemic cytokine activation that lasts for more than 4 hours (Figure S6). R848 induces robust cytokine response at the dose of 2.5 nmol/g and slightly weaker response at the dose of 5 nmol/g, thus confirming published data that the 2.5 nmol/g i.p. dose of R848 is optimal (Hemmi et al., 2002). Therefore, P3C at 3.3 nmol/g and R848 at 2.5 nmol/g were used in experiments shown in Figure 5.

EXTENDED EXPERIMENTAL PROCEDURES

Peptide Sources and Reconstitution

Peptides were synthesized by AAPPTec (Louisville, KY) or GenScript (Piscataway, NJ). Fluorescently-labeled 2R9 was supplied by ProImmune (Oxford, UK). All peptides were of 95% purity or purer. Peptide stocks were quantified spectrophotometrically (Pace et al., 1995) and stored at -80 C. Peptide sequences are shown in Table S1.

Expression Vectors

TLR4-Cer, TLR2-Cer, MyD88 TIR-Cer, and TIRAP-Cer expression vectors were described previously (Piao et al., 2013a; Piao et al., 2013b; Toshchakov et al., 2011). DNA encoding the full length TLR6 and TLR1 TIR domain was generated by PCR amplification from a mouse cDNA library using modified primers and cloned into the TLR4-Cer construct to replace the TLR4-coding sequence.

Because expression of the full length TLR1-Cer fusion was low and did not produce a sufficient donor signal, a truncated variant of TLR1-Cer fusion was used. This variant lacks the TLR1 ectodomain, but retains full transmembrane section and the TIR domain. In MyD88-Cer fusion, Cer was fused to the C terminus of MyD88 TIR domain through a short linker, replacing the intermediate and death domains of MyD88. TLR7 and TLR9 TIR coding sequences together with transmembrane region of the receptors were PCR amplified from mouse macrophage cDNA library and inserted into the pcDNA 3.1 vector in frame with C-terminal Cer.

ELISA

1×10^6 peritoneal macrophages or 2×10^5 iBMDM were plated in 24- or 12-well plates, respectively, and incubated overnight. Cells were treated with peptides for 30 min prior to LPS stimulation. Mouse TNF-α, IL-6, and IL-12 p40 were measured using ELISA kits from

Biolegend (San Diego, CA). Mouse IFN-α and IFN-β ELISA kits were from PBL Assay Science (Piscataway, NJ) and R&D Systems (Minneapolis, MN), respectively.

Immunoblotting and Co-immunoprecipitation

Expression vectors were transfected to cells using Superfect (Qiagen, CA). 48 h post-transfection, cells were lysed using buffer containing 20 mM Hepes (pH 7.4), 150 mM NaCl, 10 mM NaF, 2 mM Na_3VO_4, 1 mM EDTA, 1 mM EGTA, 0.5% Triton X-100, 0.1 mM DTT, 1 mM PMSF and protease inhibitor cocktail (Roche, Indianapolis, IN). Rabbit antibody against phospho-ERK, phospho-JNK, phospho-IKKα/β (Ser180/Ser181), MyD88, TIRAP, and GAPDH, or mouse antibody against phospho-STAT1-Y701 and STAT1 were from Cell Signaling Technology (Danvers, MA). Protein was quantified using protein quantification kit from Bio-Rad (Philadelphia, PA). Equal amount of protein was loaded and analyzed by 10% SDS-PAGE and immunoblotting. 500 μg total protein of cell extract was incubated with 1 μg of anti-mTLR2 antibody (T2.5, Santa Cruz Biotechnology, Dallas, TX) for 2 h, followed by 4 h incubation with 25 μl protein G Agarose beads (Roche). The beads were then washed 4 times with lysis buffer and boiled in Laemmli sample buffer (Bio-Rad).

Dot Blot Analysis of Peptide-Protein Binding

$2x10^6$ HEK293T cells were transfected with 10 μg of Cer-tagged full length TLR2, TLR4, or TLR6 construct or 1 μg of TLR1 TIR, MyD88 TIR, or TIRAP construct. Cells were lysed 48 hours post transfection. Lysates containing 100 μg of total protein were diluted by PBS to 500 μL and incubated with or without peptides (20 μM) for 1 h at 4 C, followed by 3 h incubation with 0.5 μg of anti-eCFP antibody (8A6, Origene, Rockville, MD) and 4 h incubation with 25 μl protein G agarose beads. The beads were washed 4 times and boiled in Laemmli sample buffer. Supernatants were spotted into PVDF membrane, followed by immunoblotting with anti-Antp

Ab (Abcam, Cambridge, MA).

Quantitative Real Time RT-PCR

Total RNA was isolated using Nucleospin RNA II kits (Macherey-Nagel, Inc. Bethlehem, PA) and treated with DNase. cDNA was synthesized from 1 µg of RNA using Goscript transcriptase (Promega), and subjected to real-time PCR with gene-specific primers for HPRT, TNF-α, IL-1β, IFN-β, and IL-6 (Couture et al., 2012) using H7900 ABI system and Fast SYBR®Green master mix (Applied Biosystems, Foster City, CA).

MTT Viability Assay

5 x 10^4 mouse peritoneal macrophages were plated into 96-well tissue culture plates, incubated overnight, and treated with peptides with or without TLR2 stimulation for 2 or 5 hours, followed by 3 h incubation with MTT (3-(4,5-Dimethylthiazol-2-yl)-2,5-diphenyltetrazolium bromide) at 0.5 mg/ml (Sigma-Aldrich). 50 µl DMSO was added to cells before reading OD at 540 nm.

FLIM

HeLa cells, transfected with a Cer-labeled protein a day before, were seeded at the density of 7000 cells/well into a 50-well gasket (Grace Bio-Labs, Bend, OR) mounted on a microscope slide. Next day, cells were treated with BTX-2R9 for 1 h and fixed. HeLa cells transfected with TLR7-TIR-Cer pcDNA 3.1 were treated with BTX-2R9 four hours after reseeding, i.e., one day after transfection, i.e., one day earlier that for the other vectors, because of fast clearance of the TLR7-TIR-encoding vector by HeLa and HEK292T host cells. FLIM images were obtained using the Alba V confocal FLIM system (ISS Inc., Champaign, IL). Cer fluorescence was excited with a 443 nm laser diode and detected through the 480/40 bandpass emission filter. FLIM images were acquired using frequency-domain modality and analyzed to fit a biexponential model of intensity decay as described previously (Szmacinski et al., 2014). Briefly,

fractional amplitudes of components were calculated on the pixel-by-pixel basis by fitting the FLIM data to the bi-exponential model with fixed lifetimes. In this model, the short lifetime component is associated with quenched donor and reflects the amount of donor-acceptor pairs, while the long lifetime component represents fluorescence of unquenched, free donor. Normalized amplitudes of components reflect relative molecular concentrations of quenched, *i.e*, acceptor-bound, and free donor molecules as α_1= [DA]/([D]+[DA]) and α_2= [D]/([D]+[DA]), where $\alpha_1+\alpha_2=1.0$

Animal Experiments

Eight week old C57BL/6J mice were injected i.p. with P3C (3.3 nmol/g of animal weight) or R848 (2.5 nmol/g). Peptides reconstituted in PBS were administered i.p. at the dose 10 nmol/g. Control group of mice received equivalent volume of PBS. The blood plasma samples were collected and kept frozen until analyzed for cytokine contents by ELISA. All animal experiments were conducted with institutional approval.

Data Representation

Numerical data are presented as means + SEM. Differences were evaluated using 1 way ANOVA and Prizm 5 software. Unless specified differently in a figure legend, asterisks mark data statistically different from the control with probability more than 99%. Significance of differences in mortality was determined by the Mantel-Cox test.

Supplemental References

Couture, L.A., Piao, W., Ru, L.W., Vogel, S.N., and Toshchakov, V.Y. (2012). Targeting Toll-like Receptor (TLR) Signaling by Toll/Interleukin-1 Receptor (TIR) Domain-containing Adapter Protein/MyD88 Adapter-like (TIRAP/Mal)-derived Decoy Peptides. J Biol Chem *287*, 24641-24648.

Guex, N., and Peitsch, M.C. (1997). SWISS-MODEL and the Swiss-PdbViewer: an environment for comparative protein modeling. Electrophoresis *18*, 2714-2723.

Hemmi, H., Kaisho, T., Takeuchi, O., Sato, S., Sanjo, H., Hoshino, K., Horiuchi, T., Tomizawa, H., Takeda, K., and Akira, S. (2002). Small anti-viral compounds activate immune cells via the TLR7 MyD88-dependent signaling pathway. Nat Immunol *3*, 196-200.

London, N., Movshovitz-Attias, D., and Schueler-Furman, O. (2010). The structural basis of peptide-protein binding strategies. Structure *18*, 188-199.

Pace, C.N., Vajdos, F., Fee, L., Grimsley, G., and Gray, T. (1995). How to measure and predict the molar absorption coefficient of a protein. Protein Sci *4*, 2411-2423.

Piao, W., Ru, L.W., Piepenbrink, K.H., Sundberg, E.J., Vogel, S.N., and Toshchakov, V.Y. (2013a). Recruitment of TLR adapter TRIF to TLR4 signaling complex is mediated by the second helical region of TRIF TIR domain. Proc Natl Acad Sci U S A *110*, 19036-19041.

Piao, W., Vogel, S.N., and Toshchakov, V.Y. (2013b). Inhibition of TLR4 signaling by TRAM-derived decoy peptides in vitro and in vivo. J Immunol *190*, 2263-2272.

Szmacinski, H., Toshchakov, V., and Lakowicz, J.R. (2014). Application of phasor plot and autofluorescence correction for study of heterogeneous cell population. Journal of biomedical optics *19*, 46017.

Toshchakov, V.U., Basu, S., Fenton, M.J., and Vogel, S.N. (2005). Differential involvement of BB loops of toll-IL-1 resistance (TIR) domain-containing adapter proteins in TLR4- versus TLR2-mediated signal transduction. J Immunol *175*, 494-500.

Toshchakov, V.Y., Fenton, M.J., and Vogel, S.N. (2007). Cutting Edge: Differential inhibition of TLR signaling pathways by cell-permeable peptides representing BB loops of TLRs. J Immunol *178*, 2655-2660.

Toshchakov, V.Y., Szmacinski, H., Couture, L.A., Lakowicz, J.R., and Vogel, S.N. (2011). Targeting TLR4 signaling by TLR4 Toll/IL-1 receptor domain-derived decoy peptides: identification of the TLR4 Toll/IL-1 receptor domain dimerization interface. J Immunol *186*, 4819-4827.

Xu, Y., Tao, X., Shen, B., Horng, T., Medzhitov, R., Manley, J.L., and Tong, L. (2000). Structural basis for signal transduction by the Toll/interleukin-1 receptor domains. Nature *408*, 111-115.